Neurobiology of Disease

Intracellular Zn^{2+} Accumulation Contributes to Synaptic Failure, Mitochondrial Depolarization, and Cell Death in an Acute Slice Oxygen–Glucose Deprivation Model of Ischemia

Yuliya V. Medvedeva,[1,2] **Bin Lin,**[1] **C. William Shuttleworth,**[3] **and John H. Weiss**[1,2]

Departments of [1]Neurology and [2]Anatomy and Neurobiology, University of California, Irvine, Irvine, California 92697, and [3]Department of Neurosciences, University of New Mexico School of Medicine, Albuquerque, New Mexico 87131

Despite considerable evidence for contributions of both Zn^{2+} and Ca^{2+} in ischemic brain damage, the relative importance of each cation to very early events in injury cascades is not well known. We examined Ca^{2+} and Zn^{2+} dynamics in hippocampal slices subjected to oxygen–glucose deprivation (OGD). When single CA1 pyramidal neurons were loaded via a patch pipette with a Ca^{2+}-sensitive indicator (fura-6F) and an ion-insensitive indicator (AlexaFluor-488), small dendritic fura-6F signals were noted after several ($\sim$6–8) minutes of OGD, followed shortly by sharp somatic signals, which were attributed to Ca^{2+} ("Ca^{2+} deregulation"). At close to the time of Ca^{2+} deregulation, neurons underwent a terminal increase in plasma membrane permeability, indicated by loss of AlexaFluor-488 fluorescence. In neurons coloaded with fura-6F and a Zn^{2+}-selective indicator (FluoZin-3), progressive rises in cytosolic Zn^{2+} levels were detected before Ca^{2+} deregulation. Addition of the Zn^{2+} chelator N,N,N′,N′-tetrakis(2-pyridylmethyl)ethylenediamine (TPEN) significantly delayed both Ca^{2+} deregulation and the plasma membrane permeability increases, indicating that Zn^{2+} contributes to the degenerative signaling. Present observations further indicate that Zn^{2+} is rapidly taken up into mitochondria, contributing to their early depolarization. Also, TPEN facilitated recovery of the mitochondrial membrane potential and of field EPSPs after transient OGD, and combined removal of Ca^{2+} and Zn^{2+} markedly extended the duration of OGD tolerated. These data provide new clues that Zn^{2+} accumulates rapidly in neurons during slice OGD, is taken up by mitochondria, and contributes to consequent mitochondrial dysfunction, cessation of synaptic transmission, Ca^{2+} deregulation, and cell death.

Key words: hippocampal slice; mitochondria; zinc; calcium; Ca^{2+}; ischemia

Introduction

Relatively short periods of cerebral ischemia can result in irreversible neuronal damage. Critical triggering mechanisms are proposed to include uncontrolled glutamate release, influx and intracellular accumulation of Ca^{2+}, and the occurrence of repetitive waves of profound neuronal depolarization (Rothman and Olney, 1986; Siesjö, 1988; Dohmen et al., 2008). A sustained rise in intracellular Ca^{2+} in neuronal somata ("Ca^{2+} deregulation") has often been considered predictive of cell death (Randall and Thayer, 1992; Nicholls and Budd, 2000; Shuttleworth and Connor, 2001; Vander Jagt et al., 2008).

Zn^{2+} is present at high concentrations in brain, where it is sequestered in presynaptic vesicles of certain excitatory pathways, and can be released into the synapse following neuronal stimulation. After ischemia or prolonged seizures, Zn^{2+} accumulates in hippocampal pyramidal neurons (Frederickson et al., 1989; Tønder et al., 1990) likely due to a combination of presynaptic Zn^{2+} release and entry into postsynaptic neurons ("translocation"), and release from stores already present within neurons. *In vitro* studies indicate that Zn^{2+} can potently disrupt mitochondrial function (Skulachev et al., 1967; Link and von Jagow, 1995; Manev et al., 1997; Brown et al., 2000; Weiss et al., 2000; Dineley et al., 2003; Gazaryan et al., 2007). In transient forebrain ischemia, observations that Zn^{2+} chelation protects hippocampal CA1 neurons implicate Zn^{2+} as a contributor to their injury (Koh et al., 1996; Calderone et al., 2004); further *in vivo* studies have suggested that Zn^{2+} may act in part via disruption of mitochondrial function following ischemia (Calderone et al., 2004; Bonanni et al., 2006).

However, as previous studies have generally examined Zn^{2+} accumulation or effects of its chelation on outcome hours to days after the ischemic event, little is known about Zn^{2+} contributions to the initiation of death cascades. These mechanisms can be studied using brain slices subjected to oxygen–glucose deprivation (OGD), a procedure that mimics some aspects of stroke. In hippocampal slice models, extracellular and intracellular Zn^{2+} levels increase shortly after onset of OGD (Wei et al., 2004; Stork and Li, 2006), and application of high concentrations of the

Zn^{2+}-selective chelator TPEN decreased subsequent cell death (Stork and Li, 2006).

In light of the ability of many Ca^{2+} indicators to detect Zn^{2+} rises (Cheng and Reynolds, 1998; Devinney et al., 2005), and recent observations suggesting that Zn^{2+} rises contributed substantially to measured fluorescence changes of a Ca^{2+} indicator in hippocampal slices subjected to OGD (Stork and Li, 2006), a key aim of present studies was to simultaneously visualize Zn^{2+} and Ca^{2+} dynamics in individual CA1 neurons in slices subjected to OGD, to clarify their respective contributions to the induction of cell death. Our studies indicate that OGD induces rapid Zn^{2+} accumulation in neurons and its uptake into mitochondria, and that the Zn^{2+} contributes to sequelae including Ca^{2+} deregulation. The Ca^{2+} deregulation contributes to a terminal loss of membrane integrity and cell death. Thus, interventions targeting neuronal Zn^{2+} accumulation and its interaction with mitochondria may offer critical benefits when delivered in the acute phases of ischemia.

Materials and Methods

Animals. Animal procedures were conducted in accordance with the National Institutes of Health *Guide for the Care and Use of Laboratory Animals* and with protocols approved by the Institutional Animal Care and Use Committee of the University of California at Irvine. Efforts were made to minimize animal suffering and number of mice used.

Preparation of acute hippocampal slices. Hippocampal slices were prepared from 4-week-old Swiss Webster mice (Hilltop Lab Animals). Mice were deeply anesthetized with isoflurane and decapitated, and the brain was rapidly removed. Hippocampal slices (300 μm) were cut with a vibratome (VT-1200, Leica Microsystems) in chilled cutting solution, containing (in mM) 3 KCl, 1.25 NaH_2PO_4, 0.2 $CaCl_2$, 6 $MgSO_4$, 26 $NaHCO_3$, 220 sucrose, 10 glucose, and 0.43 ketamine (pH 7.35, 310 mOsm, equilibrated with 95% O_2/5% CO_2) and then transferred into artificial CSF (ACSF) containing (in mM) 126 NaCl, 3 KCl, 1.25 NaH_2PO_4, 2 $CaCl_2$, 1 $MgSO_4$, 26 $NaHCO_3$, and 10 glucose (pH 7.35, 310 mOsm, adjusted with sucrose and equilibrated with 95% O_2/5% CO_2). After preincubation for 1 h at 34°C, all slices were placed in a holding chamber at room temperature for at least 1 h before being transferred to a recording chamber; throughout, slices were submerged in ACSF.

Loading individual hippocampal CA1 neurons with fluorescent indicators and fluorescence measurements. For recordings slices were placed in a flow-through chamber (RC-27L chamber with plastic slice anchor (Warner Instruments) mounted on the stage of an upright microscope (BX51WI, Olympus) and superfused with oxygenated ACSF (95% O_2/5% CO_2) at 2 ml/min. Experiments were performed at 32 ± 0.5°C. Whole-cell patch-clamp recordings were obtained using a patch-clamp amplifier (Axopatch 200B) and an analog-to-digital converter Digidata 1322A (Molecular Devices). Patch pipettes (5–7 MΩ) were pulled from borosilicate glass with filament (World Precision Instruments) on a P-87 micropipette puller (Sutter Instruments) and filled with the following solution (mM): 125 K-gluconate, 10 KCl, 3 Mg-ATP, 1 $MgCl_2$, 10 HEPES, pH 7.25 with KOH (290 mOsm with sucrose). Fluorescent indicators were dissolved in pipette solution (FluoZin-3, 1 mM; fura-6F, 1 mM; AlexaFluor-488, 0.5 mM) and loaded into the pipette tip (1 μl) before backfilling with pipette solution. Neurons were loaded with fluorescent indicators via patch pipettes by holding neurons in the whole-cell configuration at −60 mV for ~5 min. The pipettes were then slowly withdrawn from the cell. This technique of loading with a small volume of concentrated indicator in the pipette tip is similar to that used and discussed in a recent study (Vander Jagt et al., 2008) and provides the benefit of good loading of dendritic processes while minimizing cellular dialysis. Successful pipette removal was judged by monitoring both the formation of an outside-out patch and Ca^{2+} levels in neuronal somata. If the patch was formed successfully (leakage current less then 30 pA) and $[Ca^{2+}]_i$ did not increase, cells were considered healthy and used for experiment after a 30 min recovery.

For simultaneous measurements of intracellular Ca^{2+} and Zn^{2+} dy-

namics cells were coloaded with the low-affinity Ca^{2+}-sensitive indicator fura-6F ($K_{d_{Ca}}$ ~5.3 μM), and the high-affinity Zn^{2+}-sensitive indicator FluoZin-3 ($K_{d_{Zn}}$ ~15 nM). To assess changes in membrane integrity, the ion-insensitive indicator AlexaFluor-488 hydrazide was coloaded with fura-6F. Fluorescence was alternately excited at 340 (20), 380 (20), and 482 (20) nm via a 40× water-immersion objective [numerical aperture (NA) 0.8, Olympus], using a xenon light source (Sutter Instruments), and emission collected at 532 (40) nm using a CCD camera (Hamamatsu). (All filters are bandpass with bandwidths indicated in parentheses.) Images were acquired at 5 or 30 s intervals and analyzed, after background subtraction, with METAFLUOR 7.0 software (Molecular Devices). For figure presentation, background-subtracted 340/380 ratio images were masked using the 482 nm AlexaFluor-488 images (if available) or the 380 nm fluorescent images. $[Ca^{2+}]_i$ values are presented as the 340/380 nm ratio, and $[Zn^{2+}]_i$ changes are presented as $\Delta F/F_0 = (F − F_0)/F_0$, where F is the current fluorescence intensity and F_0 is the baseline fluorescence intensity. AlexaFluor-488 changes are presented as F/F_0.

To access changes in mitochondrial potential ($\Delta\Psi_m$) slices were bulk loaded with the $\Delta\Psi_m$-sensitive probe, Rhodamine 123 (Rh123, 26 μM, 30 min at 22–25°C) before OGD and regions of interest monitored in the CA1 pyramidal cell layer and in the apical dendritic fields. This charged rhodamine derivative is taken up into polarized mitochondria, and when sufficient concentrations are used, fluorescence is quenched; under these conditions upon loss of $\Delta\Psi_m$ the dye is released from mitochondria into the cytosol and cytosolic fluorescence increases (Duchen et al., 2003). Rh123 was excited at 540 (25) nm, emitted fluorescence was collected at 605 (55) nm, and images were collected at 0.03 Hz. Data are presented as $\Delta F/F_0 = (F − F_0)/F_0$, where F is the current fluorescence intensity and F_0 is the baseline fluorescence.

Extracellular recording. Field EPSPs (fEPSPs) were recorded from CA1b stratum radiatum by using a single glass pipette (2–3 MΩ). Slices were superfused at 1.2 ml/min (32°C), and experiments were performed at 32 ± 0.5°C. Orthodromic stimulation was delivered in the Schaffer collateral–commissural projections. Pulses were administered to the stimulating electrode at 0.05 Hz using a current that elicited a 50% maximal response. Extracellular evoked responses and DC potential shifts (to assess spreading depression-like events) were recorded by a DC amplifier (A-M System). Data were stored and analyzed using the PCLAMP software (Molecular Devices) via a 16-bit data acquisition system (Digidata 1320A or 1322A, Molecular Devices) at a sampling rate of 5 kHz (fEPSP) or 1 kHz (DC potential).

Oxygen–glucose deprivation in slices and nominally Ca-free experiments. To simulate hypoxic-hypoglycemic conditions ACSF was replaced with identical solution but lacking glucose (glucose was substituted with an equimolar concentration of sucrose) and equilibrated with 95% N_2/5% CO_2. For Ca^{2+} removal, Ca^{2+} was substituted with 2 mM Mg^{2+} (Ca-free ACSF).

Reagents. N,N,N′,N-tetrakis(2-pyridylmethyl)ethylenediamine (TPEN) 20 mM stock solution was made freshly every day in 95% ethanol and then diluted to final concentration of 40 μM in ACSF. Carbonylcyanide-4-(trifluoromethoxy)-phenylhydrazone (FCCP) was used at 5 μM prepared from 10 mM stock (in DMSO). Fura-6F, FluoZin-3, bis-fura-2, and AlexaFluor-488 were obtained from Invitrogen. FCCP was purchased from Tocris Bioscience. All other reagents were purchased from Sigma.

Data analysis. In OGD experiments FluoZin-3 fluorescence decreased slightly due to photobleaching. To determine the onset of OGD-induced Zn^{2+} rises, the baseline was linearly fitted and the Zn^{2+} rise onset determined as the intersection of this line with a linear extrapolation of the maximum slope of the first Zn^{2+} rise exceeding 20% over baseline. The onset time of Ca^{2+} deregulation, was determined from the intersection of the linear extrapolation of the baseline and a linear fit of the maximum slope of the fura-6F ratio 340/380 increase as it rose ≥6-fold. Differences between groups were tested using Student's *t* test (or paired *t* test as indicated). All comparisons reflect sets of data substantially interleaved in time, and were based on 4–10 slices from ≥4 animals each condition (numbers of cells and slices are indicated for each expt).
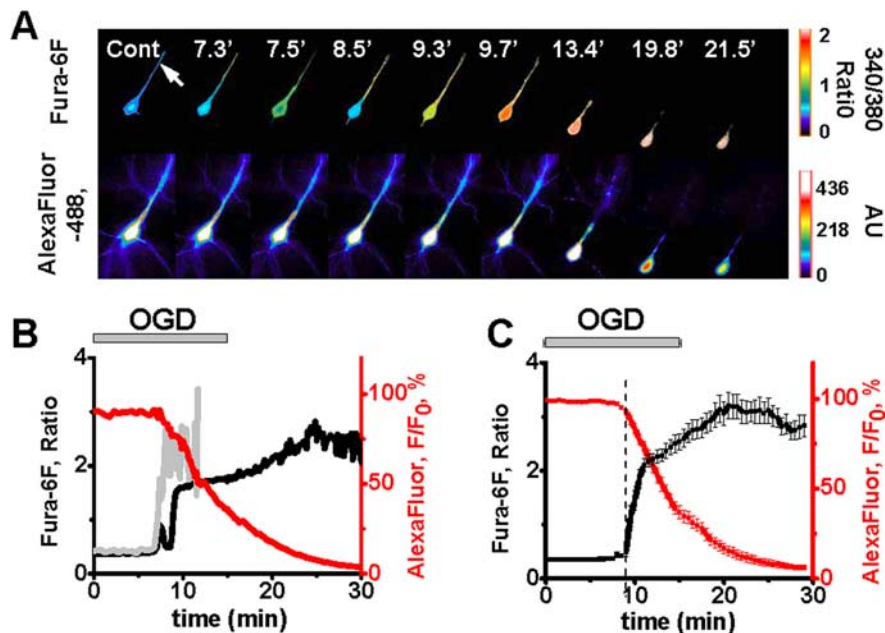
Figure 1. OGD induces Ca^{2+} deregulation followed by loss of membrane integrity in CA1 neurons. ***A***, Fluorescence images of an individual CA1 neuron coloaded via a patch pipette with a ratiometric Ca^{2+}-sensitive indicator (top panels; 340/380 nm fura-6F ratio images) and an ion-insensitive fluorescent marker (bottom panels; AlexaFluor-488 fluorescence). Arrow indicates the location of the dendritic measurements, and numbers indicate time (in minutes) following onset of OGD. ***B***, Traces show somatic fura-6F ratio (black) and AlexaFluor-488 (red) fluorescence changes in the same neuron illustrated in ***A***. The gray trace shows the fura-6F changes in the dendrite. ***C***, Traces show mean fluorescence changes ($\pm$SEM) from the somata of 10 CA1 neurons (black: fura-6F ratio, red: AlexaFluor-488). Individual responses have been aligned to the onset of an irrecoverable fura-6F ratio increases ("Ca^{2+} deregulation") in each neuron (dashed line, 9.0 $\pm$ 0.34 min). The OGD bar shows the time of OGD exposure ($\pm$SEM). Note the abrupt acceleration in the loss of AlexaFluor-488 fluorescence, indicative of a terminal loss of membrane integrity, starting close to the time of Ca^{2+} deregulation.

Results

Ca^{2+} deregulation and loss of membrane integrity in CA1 neurons during OGD

A number of past studies have examined contributions of Ca^{2+} accumulation to hippocampal neuronal injury in slice OGD models of ischemia (Lobner and Lipton, 1993; Tanaka et al., 1997; Lipski et al., 2006). Our first aim was to ascertain the specific relationship between cytosolic Ca^{2+} increases in individual CA1 neurons subjected to OGD, and the occurrence of irreversible injury as indicated by a loss of membrane integrity. CA1 pyramidal neurons were loaded via patch pipettes with the low-affinity Ca^{2+}-sensitive indicator, fura-6F and an ion-insensitive fluorescent compound, AlexaFluor-488 (see Materials and Methods). After removal of the loading pipette, cells were monitored for ~40 min, and if baseline Ca^{2+} levels appeared stable, subjected to 15 min of oxygen–glucose deprivation (OGD).

Approximately 6–10 min following the onset of OGD, fura-6F ratio increases were noted to begin within apical dendrites (sometimes with an associated small transient rise in the soma), followed within 1–3 min by large abrupt fura-6F increases in somata ("Ca^{2+} deregulation"; onset at 9.0 $\pm$ 0.34 min, $n = 10$ cells from 8 slices, 8 mice) (Fig. 1). Somatic Ca^{2+} deregulation was always accompanied by the onset of a severe loss of AlexaFluor-488 fluorescence, and there was no recovery of fura-6F ratio after this time point. These data are indicative of an increase in membrane permeability and loss of neuronal viability (Randall and Thayer, 1992; Vander Jagt et al., 2008). In another set of slices, an extracellular recording electrode was placed in the adjacent dendritic fields to assess the occurrence of a spreading depression (SD)-like event (Dietz et al., 2008). In 4 slices in which

SD was recorded while monitoring Ca^{2+} rises in individual CA1 neurons, the SD (peak at 7.27 $\pm$ 0.92 min) always preceded the initial dendritic Ca^{2+} rise (at 8.18 $\pm$ 1.03 min; $p < 0.05$ by paired t test).

Although we refer to the irrecoverable fura-6F ratio increases described above as a "Ca^{2+} deregulation" event, in light of previous studies reporting that Zn^{2+} may contribute substantially to Ca^{2+} indicator signals during OGD, we performed additional ion substitution (Ca^{2+} removal) and Zn^{2+} chelation studies to further clarify the ionic basis of the event, and its contribution to the induction of the terminal loss of membrane integrity. First, we performed prolonged (30 min) OGD exposures in nominally Ca^{2+}-free ACSF, monitoring neuronal fura-6F and AlexaFluor-488 fluorescence changes as above. Superfusion with Ca^{2+}-free ACSF was started 5 min before the OGD, and slices were reexposed to normal ACSF (with 2 mM Ca^{2+}) 5 min after the OGD exposure was terminated. Under these conditions, there was either no demonstrable fura-6F ratio change throughout the OGD, or (in 4/8 cells) there was a small ratio increase (<1) between 25 and 30 min of OGD. There was also a slow decrease in AlexaFluor-488 fluorescence throughout the OGD which seemed to be due to enhanced cell swelling upon OGD in the absence of Ca^{2+} ions, causing dilution of the signal. However, in all neurons, Ca^{2+} deregulation (with >6-fold ratio increase) and an associated sharp acceleration of AlexaFluor-488 fluorescence loss occurred almost immediately following restoration of 2 mM Ca^{2+} (after 1.5 $\pm$ 0.58 min, $n = 8$ cells, 8 slices, 8 mice) (Fig. 2A). These results support a direct contribution of Ca^{2+} to the loss of membrane integrity, much as was recently reported in a study of prolonged excitotoxic activation (Vander Jagt et al., 2008). Furthermore, these data are consistent with the idea that large increases in cytosolic Ca^{2+} (rather than Zn^{2+}) are responsible for the abrupt and irrecoverable fura-6F signal increases. However, it remained possible that intracellular Zn^{2+} could accumulate (and then bind to fura-6F) in a manner that was dependent on extracellular Ca^{2+}.

To test this possibility, we examined the effects of a high-affinity chelator of Zn^{2+} (TPEN, 40 μM; 15 min preexposure and present throughout OGD) on fura-6F signals during OGD. (Of note, although TPEN is routinely used as a Zn^{2+} chelator, it can bind other metals including Cu^{2+} and Fe^{2+}, and we cannot rule out that interactions with these trace metals could contribute to its effects.) Under these conditions, irrecoverable fura-6F increases still occurred, but were significantly delayed [occurring at 15.45 $\pm$ 0.77 min, $n = 12$ cells from 9 slices, 8 mice (Fig. 2B), compared with 9.0 $\pm$ 0.34 min in the absence of TPEN (Fig. 1C), $p < 0.001$], and were still closely linked to an irrecoverable increase in plasma membrane permeability. Thus, the occurrence of this event despite the presence of a Zn^{2+} chelator supports the inference that Ca^{2+} is the primarily ionic contributor to the large fura-6F signals (which will be referred to below as "Ca^{2+} deregulation" events).
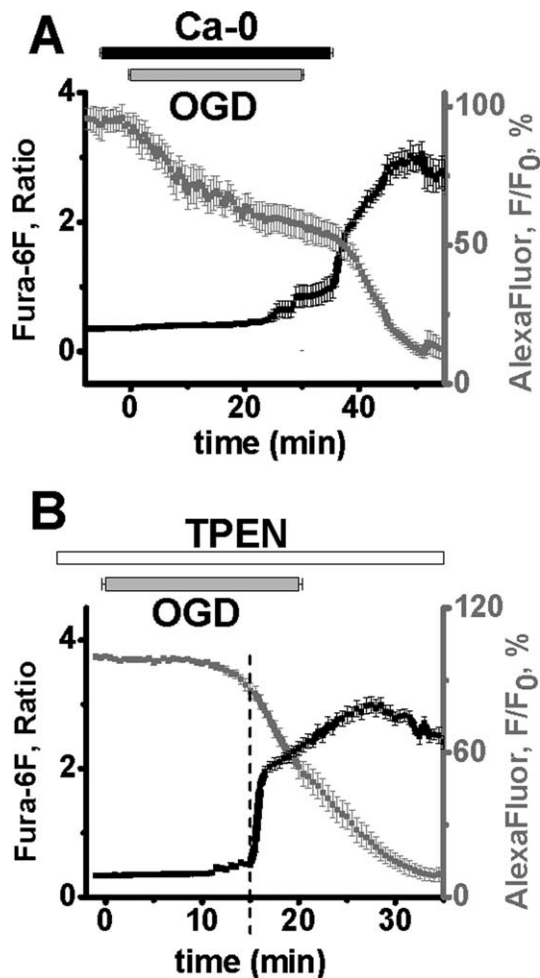
Figure 2. Zn^{2+} and Ca^{2+} contribute to OGD-induced damage of CA1 pyramidal neurons. **A**, Ca^{2+} removal during OGD prevents the Ca^{2+} deregulation. CA1 neurons were loaded with fura-6F (black) and AlexaFluor-488 (gray). Slices were superfused with Ca^{2+}-free ACSF for 5 min before, during, and for 5 min after a 30 min episode of OGD. In cells exposed to OGD for 30 min, Ca^{2+} deregulation occurred almost immediately (1.5 ± 0.6 min, $n = 8$) after restoration of Ca^{2+} to the media, and as previously observed with Ca^{2+} containing ACSF, was accompanied by an abrupt acceleration in the rate of AlexaFluor-488 fluorescence loss, indicative of a terminal loss of membrane integrity. The slow loss of AlexaFluor-488 fluorescence throughout the OGD appeared to be largely attributable to enhanced cell swelling during zero-Ca^{2+} OGD. Individual responses (±SEM) have been aligned to the onset of Ca^{2+} deregulation, and the OGD bar shows the time of OGD exposure (±SEM), as above. **B**, TPEN significantly delays OGD-evoked Ca^{2+} deregulation. Neurons were loaded with fura-6F (black) and AlexaFluor-488 (gray), and exposed to TPEN (40 μM) before and during OGD exposure in normal Ca^{2+} containing ACSF ($n = 12$). Fura-6F signal increases and loss of membrane integrity (indicated by loss of AlexaFluor-488 fluorescence) (±SEM) still occurred, but were significantly delayed compared with responses in normal ACSF (see Fig. 1C). Individual responses have been aligned to the onset of Ca^{2+} deregulation, and the OGD bar shows the time of OGD exposure (±SEM), as above.

Although TPEN is a very weak Ca^{2+} chelator (K_d ~4×10^{-5} M) (Arslan et al., 1985), additional control experiments were performed to verify that the TPEN exposures used did not substantially buffer intracellular Ca^{2+} rises. CA1 neurons were loaded with the relatively high-affinity Ca^{2+} indicator bis-fura-2 (K_d ~370 nM) and subjected to step depolarizations (from −60 to 0 mV, 1 s) before, after 10 min exposure to, and after 10 min washout of 40 μM TPEN. TPEN had no significant effect on the magnitude of the bis-fura-2 ratio increase (ctrl: 100 ± 6.7%; TPEN: 84.5 ± 9.1%; washout: 74.3 ± 5.9%; ctrl vs TPEN $p = 0.33$, $n = 4$). Thus, TPEN has little effect on depolarization-induced Ca^{2+} rises, which were far lower than those we detect with fura-6F, and

the delay of Ca^{2+} deregulation-induced by TPEN is most likely due to Zn^{2+} chelation.

Slow Zn^{2+} rises generally precede and contribute to the induction of the Ca^{2+} deregulation

We next set out to measure OGD-induced changes in intracellular Zn^{2+} levels in relationship to the time of Ca^{2+} deregulation. OGD exposures (15 min) were performed as above, but after loading individual CA1 neurons with fura-6F along with a Zn^{2+} selective indicator (FluoZin-3) (Gee et al., 2002). A similar approach was recently reported to enable discrimination between Ca^{2+} and Zn^{2+} rises in cultured neurons (Devinney et al., 2005) and in hippocampal slices (Dietz et al., 2008). Under these conditions, a slow and progressive increase in somatic FluoZin-3 fluorescence began 5–10 min after onset of OGD (starting at 7.74 ± 0.23 min; 9 cells from 8 slices, 5 mice), which was followed at 10.27 ± 0.32 min by Ca^{2+} deregulation (Fig. 3). Notably, the initial slow Zn^{2+} rise preceded the Ca^{2+} deregulation in all cells examined, and generally preceded even the initial dendritic fura-6F signals (which occurred at 8.8 ± 0.51 min; $p < 0.05$ vs Zn^{2+} rise by paired t test). After the sharp signal increases in both indicators there was a loss of FluoZin-3 fluorescence, likely reflecting loss of indicator from cells. Indeed, while the fura-6F ratio remained high, the absolute fluorescence signals for this indicator progressively decreased at both 340 and 380 nm wavelengths, indicative of membrane disruption as previously described (Vander Jagt et al., 2008). Finally, to further confirm that the FluoZin-3 signal does indeed represent a cytosolic Zn^{2+} rise, neurons were loaded with FluoZin-3 and fura-6F as above, and exposed to OGD in the presence of TPEN. Preexposure of slices to TPEN caused a substantial drop in basal FluoZin-3 fluorescence (80 ± 3.2% in 10 min; 6 cells from 5 slices, 4 mice), and virtually eliminated FluoZin-3 signals seen during OGD (Fig. 4A), while having little effect on the Ca^{2+} deregulation (other than it being delayed compared with control). Thus, these observations support the idea that slow cytosolic Zn^{2+} rises precede and contribute to the occurrence of Ca^{2+} deregulation, which in turn is linked to loss of membrane integrity and cell death.

Additional experiments were performed to resolve the contribution of the Zn^{2+} increase to Ca^{2+} deregulation. First, to investigate the dependence of the early Zn^{2+} rise upon influx of Ca^{2+} ions, CA1 neurons were loaded with FluoZin-3 and fura-6F and subjected to OGD for 30 min in nominally Ca^{2+}-free ACSF (Fig. 4B). Under these conditions, FluoZin-3 fluorescence increases still occurred between 5 and 10 min, although they were blunted, and as described above for AlexaFluor-488 in the case of zero-Ca^{2+} OGD exposures, were followed by slow fluorescence decreases due to neuronal swelling (see Fig. 2). Also, as in Figure 2A, a small fura-6F signal was noted in some (3/7, 6 slices, 6 mice) cells during the OGD, and Ca^{2+} deregulation occurred very shortly after restoration of Ca^{2+} to the ACSF (1.73 ± 0.65 min) (Fig. 4B).

Cumulative results above suggest that a Zn^{2+} rise occurring after several min of OGD contributes to the induction of Ca^{2+} deregulation, which in turn is causally linked to a loss of membrane integrity. To further clarify the role of each of these ions in the subsequent cell death, we loaded CA1 neurons with fura-6F and AlexaFluor-488, and performed 30 min OGD exposures in which both cations were transiently removed (Ca^{2+}-free ACSF + TPEN). Under these conditions, the Ca^{2+} deregulation was still linked to a sharp decrease in AlexaFluor-488 fluorescence, but was markedly delayed, occurring 14.24 ± 1.55 min after Ca^{2+} replacement ($n = 7$ cells from 6 slices, 6 mice vs 1.5 ± 0.58 min in
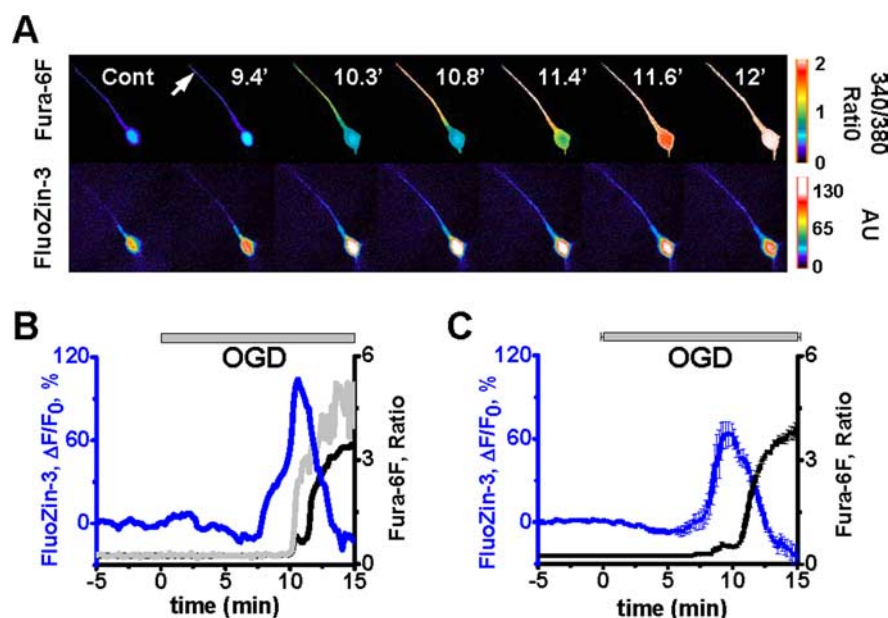
Figure 3. OGD-evoked Zn²⁺ rises precede the Ca²⁺ deregulation. **A**, Fluorescence images of an individual CA1 neuron coloaded via a patch pipette with a ratiometric Ca²⁺-sensitive indicator (top panels; 340/380 nm fura-6F ratio images) and a Zn²⁺ selective indicator (bottom panels; FluoZin-3). Arrow indicates the location of the dendritic measurements, and numbers indicate time (in minutes) following onset of OGD. **B**, Traces show somatic FluoZin-3 fluorescence (blue) and fura-6F ratio (black) changes in the same neuron illustrated in **A**. The gray trace shows the fura-6F changes in the dendrite. **C**, Traces show mean somatic FluoZin-3 fluorescence (blue) and fura-6F ratio (black) changes from 9 CA1 neurons, and are aligned for the onset of the Ca²⁺ deregulation. The OGD bar shows the time of OGD exposure (±SEM). The onset of the Zn²⁺ rise (7.74 ± 0.23 min) preceded the Ca²⁺ deregulation (10.27 ± 0.32 min) in all neurons.

control, $p < 0.001$) (Fig. 4C). Thus, the ability of TPEN to significantly delay the degenerative events regardless of the presence of extracellular Ca²⁺ suggests an important role for Zn²⁺ accumulation during the period of OGD in the initiation of the injury response.

Zn²⁺ and Ca²⁺ both contribute to an irreversible loss of synaptic transmission

We next examined the contribution of Zn²⁺ to a functional consequence of OGD, specifically the failure of synaptic transmission, by recording presynaptic fiber volleys and field EPSPs (fEPSPs) evoked by Schaffer collateral afferent stimulation (Fig. 5). For initial studies, we selected OGD exposure times of 10 min, which is modestly longer than the time to Ca²⁺ deregulation in the absence of TPEN (9.0 ± 0.34 min), with the expectation that this exposure would likely produce loss of synaptic function, while allowing a good chance of rescue by Zn²⁺ chelation. Of note, as it likely takes 1–2 min after restoration of normal ACSF to reverse the effects of OGD, the effective duration of this insult is likely somewhat longer. Presynaptic fiber volleys decreased by >90% within several min of OGD, but largely recovered (to 64.6 ± 9.23% of baseline, $n = 9$) within 30 min after the OGD exposure. Postsynaptic responses were also promptly depressed, but unlike presynaptic signals, fEPSPs showed no significant recovery over the time course assessed (5.7 ± 3.65% of baseline at 8 min of OGD, 6.8 ± 2.81% of baseline after 1 h reperfusion). TPEN (40 μM) had no effect on basal transmission (presynaptic fiber volley or fEPSP amplitude), the loss or recovery of the fiber volley, or the initial loss of the fEPSP amplitude; however it markedly enhanced the recovery of the fEPSP after slices were reexposed to normal ACSF (to 59.3 ± 10.16%, of baseline within 1 h, $n = 11$, $p < 0.001$) (Fig. 5B). In contrast, with 15 min OGD, there

was no recovery in the fEPSP regardless of the presence of TPEN (data not shown), likely consistent with the occurrence of Ca²⁺ deregulation at close to 15 min of OGD when TPEN was present (Fig. 2B).

To investigate interactions between Zn²⁺ and Ca²⁺ in the loss of synaptic transmission, we next examined the effects of Ca²⁺ removal during the 15 min OGD (see Materials and Methods). Similar Ca²⁺ removal has been found to enhance recovery of synaptic transmission after transient NMDA exposure (Hoskison and Shuttleworth, 2006). Under these conditions the transient loss and recovery of the presynaptic fiber volley was largely unaffected. Notably, the perfusion of Ca²⁺-free ACSF caused >70% loss of the fEPSP even before onset of the OGD, and >97% loss at the end of the 15 min OGD. The fEPSP partially recovered within 1 h after the OGD (to 24.5 ± 7.40.6% of baseline, $n = 11$). However, when TPEN was added with the Ca²⁺-free ACSF, the recovery of the fEPSP was substantially improved (to 70.6 ± 8.97%, $n = 14$, $p < 0.001$) (Fig. 5C). In control experiments, transient exposures to Ca²⁺-free ACSF caused no significant lasting loss of either the fiber volley or the fEPSP (data not shown). Thus, with this longer 15 min episode of OGD, both Zn²⁺ and Ca²⁺ seem to contribute critically to the irreversible loss of synaptic function.

OGD induces Zn²⁺ uptake into mitochondria

We tested the hypothesis that OGD-evoked cytosolic Zn²⁺ rises are buffered by uptake into mitochondria, and that these organelles might be a crucial site of the initial deleterious effects of Zn²⁺. To examine possible Zn²⁺ uptake into mitochondria, slices were briefly preexposed to the mitochondrial uncoupler, FCCP (5 μM, 5 min). FCCP dissipates the proton gradient across the inner mitochondrial membrane, resulting in loss of the mitochondrial potential ($\Delta\Psi_m$), thereby impairing electrogenic uptake of Zn²⁺ into mitochondria and also inducing release of Zn²⁺ already present in mitochondria (Sensi et al., 2002, 2003). Under these conditions, cytosolic Zn²⁺ rises were significantly accelerated, occurring in most cells within the first minute of OGD ($n = 10$ cells, from 10 slices, 8 mice, 0.79 ± 0.50 vs 7.9 ± 0.44 min, $n = 9$ control cells matched in time, $p < 0.001$) (Fig. 6A,B). Although FCCP can induce proton flux across any membranes, FCCP alone (5 min, without subsequent OGD) caused no significant rise in Zn²⁺ or Ca²⁺ during the exposure or over the ensuing 10 min ($n = 6$ cells, 6 slices, 6 mice, data not shown), but does cause prompt loss of $\Delta\Psi_m$ (see Fig. 7, below). Thus, the accelerated cytosolic Zn²⁺ rise most likely is due to diminished uptake into mitochondria, thereby revealing cellular accumulation of free Zn²⁺ to occur very rapidly after onset of OGD. Under these conditions, the Ca²⁺ deregulation was also accelerated by FCCP, occurring 5.3 ± 0.38 min from OGD onset ($n = 10$, vs 10.1 ± 0.56, $n = 9$ control cells matched in time, $p < 0.001$). Furthermore, in cells loaded with fura-6F and AlexaFluor-488, and exposed to FCCP before OGD, the Ca²⁺ deregulation (at 4.9 ± 0.29 min, $n = 10$, 9 slices, 8 mice) (Fig. 6C) was still asso-
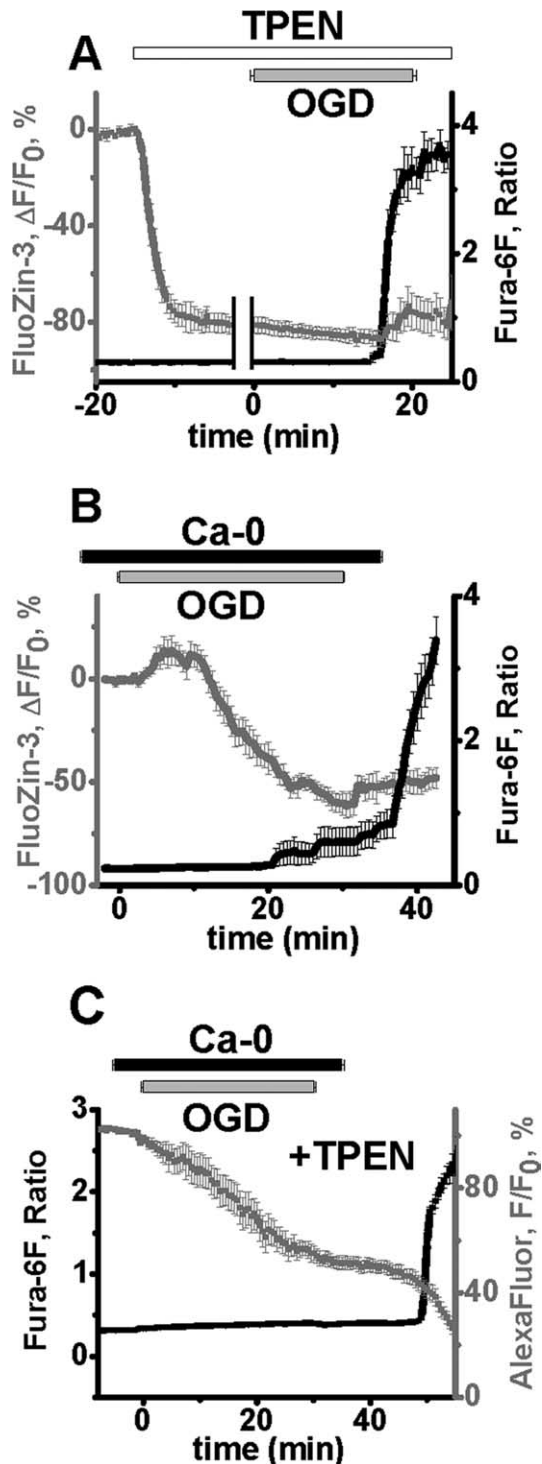
Figure 4. Ca^{2+} and Zn^{2+} both are involved in triggering of OGD evoked Ca^{2+} deregulation. **A**, Bath application of TPEN effectively chelates intraneuronal Zn^{2+} and significantly delays OGD-evoked Ca^{2+} deregulation. Neurons were coloaded with FluoZin-3 and fura-6F, and exposed to TPEN (40 μM) for 15 min before and during OGD. TPEN decreased basal FluoZin-3 fluorescence by 80 $\pm$ 3.2% within 10 min of application (gray), without affecting the fura-6F 340/380 nm ratio (black) (left side of panel; traces aligned to the addition of TPEN). Subsequent OGD exposures evoked Ca^{2+} deregulation (as indicated by a sharp fura-6F ratio increase), which was significantly delayed ($n = 6$, 16.0 ± 0.91 vs 10.27 ± 0.32 min in control, $n = 9$), but greatly reduced changes in FluoZin-3 fluorescence (which remained well below basal fluorescence) (right side of panel; traces aligned to onset of Ca^{2+} deregulation). All data ($\pm$SEM) are obtained from the same 6 CA1 neurons. **B**, OGD-induced Zn^{2+} rises still occur despite removal of extracellular Ca^{2+}. Neurons were coloaded with FluoZin-3 and fura-6F and slices superfused with Ca^{2+}-free ACSF for 5 min before, during and for 5 min after a 30 min episode of OGD. During prolonged OGD in Ca^{2+}-free ACSF, Zn^{2+} rises still occurred after 5–10

ciated with an acceleration in loss of AlexaFluor-488 fluorescence.

Interestingly, despite the acceleration of both the cytosolic Zn^{2+} accumulation and the Ca^{2+} deregulation after FCCP exposure, the interval between the onset of the Zn^{2+} rise and the Ca^{2+} deregulation was significantly increased (control, 2.1 ± 0.33 min; FCCP, 4.5 ± 0.59 min, $n = 9$ and 10 cells, $p < 0.005$). Furthermore, in the presence of FCCP, addition of TPEN did not significantly affect the time of Ca^{2+} deregulation (occurring at 5.5 ± 0.55 min, $n = 4$, 4 slices, 4 mice compared with 4.8 ± 0.38 min, $n = 5$ for matched in time control cells, 5 slices, 5 mice, $p = 0.36$), suggesting that in this case the acceleration of Ca^{2+} deregulation was not due to Zn^{2+}, and thus was likely due to direct effects of FCCP on mitochondrial function. These data suggest that Zn^{2+} accumulation within the mitochondria may be more effective than cytosolic Zn^{2+} at triggering the Ca^{2+} deregulation, and thus lend support to functional significance of the mitochondrial Zn^{2+} accumulation.

Zn^{2+} contributes to a progressive mitochondrial depolarization during OGD

Rhodamine 123 (Rh123) was used to assess changes in $\Delta\Psi_m$ during OGD (see Materials and Methods). During 15 min OGD exposures, an initial fluorescence increase began shortly after onset of OGD and was followed after several minutes by a distinct acceleration in fluorescence increase (Fig. 7A) (Bahar et al., 2000). Compared with control slices, TPEN significantly slowed the initial phase of the Rh123 fluorescence increase ($\Delta F/F_0$ increase from 2 to 5 min of $16.3 \pm 3.21\%$ in controls vs $8 \pm 1.41\%$ with TPEN, $n = 9$ and 9 slices, $p < 0.05$) and also decreased the peak $\Delta\Psi_m$ changes ($107.3 \pm 7.35\%$ in control, and $73.0 \pm 6.96\%$ with TPEN, $n = 10$ and 10, $p < 0.01$), but did not alter the time to peak $\Delta\Psi_m$ change (8.8 ± 0.52, control, 9.0 ± 0.34, TPEN, $p = 0.75$) (Fig. 7B,C). Thus, Zn^{2+} appears to contribute to the initial loss of $\Delta\Psi_m$ during OGD, consistent with evidence that it accumulates within mitochondria during OGD.

Finally, to address the ability of mitochondria to recover after a 15 min period of OGD, Rh123-loaded slices were allowed to recover for ~35 min after OGD, and then exposed to FCCP, to directly induce a loss of $\Delta\Psi_m$. In control slices, there was little $\Delta\Psi_m$ change after FCCP, suggesting that the mitochondria were already depolarized (Fig. 7B). However, in the slices exposed to OGD in the presence of TPEN, FCCP induced a substantial ΔF, suggesting that Zn^{2+} chelation during OGD permitted considerable recovery of the $\Delta\Psi_m$ after OGD (Fig. 7C).

Discussion
Neuronal Zn^{2+} rises are early triggers of the ischemic neurodegenerative cascade
Although many past studies have highlighted critical roles of Ca^{2+} entry in the induction of ischemic neuronal injury, other

←

min (as in the presence of Ca^{2+}) (Fig. 3). However, under these conditions the peak FluoZin-3 fluorescence increase seemed to be blunted, followed by a slow decrease in fluorescence due to enhanced cell swelling which occurred during OGD exposures in Ca^{2+}-free ACSF. The Ca^{2+} deregulation occurred shortly after replacement of Ca^{2+}, and was unaccompanied by major changes in the FluoZin-3 fluorescence. Traces show mean values $\pm$ SEM. **C**, TPEN significantly delays the Ca^{2+} deregulation after prolonged OGD in Ca^{2+}-free ACSF. CA1 neurons were subjected to OGD in nominally Ca^{2+}-free ACSF as in Figure 2A, but in the presence of TPEN (40 μM). Under these conditions the Ca^{2+} deregulation and associated abrupt loss of AlexaFluor-488 fluorescence still occurred, but were markedly delayed (14.2 ± 1.5 min after Ca^{2+} replacement, $p < 0.001$ vs no TPEN condition; $n = 7$ cells, $\pm$SEM).
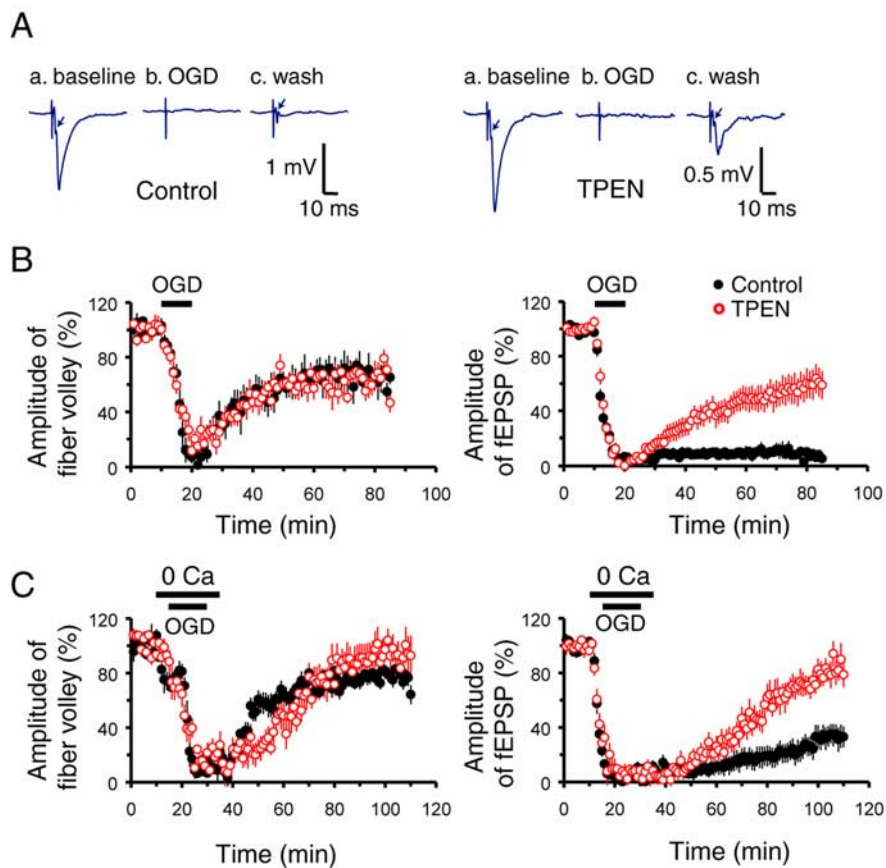
Figure 5. Ca^{2+} and Zn^{2+} both contribute to the loss of synaptic transmission after OGD. Extracellular stimulating and recording electrodes were placed in the Schaffer collateral pathway and stimuli delivered every 20 s, before, during, and after OGD. **A**, Representative traces at baseline, at the end of a 10 min period of OGD, and after 30 min recovery, in the absence (left) and presence (right) of TPEN. Arrow shows the presynaptic fiber volley, preceding the fEPSP. Note that TPEN enhances recovery of the fEPSP. **B**, Zn^{2+} contributes to the loss of synaptic transmission with 10 min OGD. OGD caused a rapid loss of both the presynaptic fiber volley (left) and the fEPSP (right). Note that the fiber volley recovered regardless of the presence of TPEN, but that the fEPSP did not recover unless TPEN was present. **C**, Zn^{2+} also contributes to the loss of synaptic transmission with longer (15 min) OGD in Ca^{2+}-free ACSF. With 15 min OGD in normal ACSF, there was no recovery of the fEPSP regardless of the presence of TPEN (data not shown). To examine possible interactions between Zn^{2+} and Ca^{2+} in the loss of transmission, slices were perfused with Ca^{2+}-free ACSF for 5 min before and after a 15 min episode of OGD. As above, OGD caused a rapid loss of both the presynaptic fiber volley (left) and the fEPSP (right), with the fiber volley recovering regardless of the presence of TPEN, but recovery of the fEPSP greatly improved in the presence of TPEN. Thus, with this longer period of OGD, both Ca^{2+} and Zn^{2+} contribute to the irreversible loss of transmission. All traces show normalized amplitudes ± SEM.

studies have emphasized apparent contributions of Zn^{2+} (Tønder et al., 1990; Koh et al., 1996; Yin et al., 2002; Calderone et al., 2004), and have demonstrated early neuronal Zn^{2+} accumulation during OGD (Wei et al., 2004). Furthermore, as discussed above, it was recently suggested that Zn^{2+} might actually mediate some effects previously attributed to Ca^{2+} (Stork and Li, 2006).

The present study, which is the first to simultaneously track changes in Zn^{2+} and Ca^{2+} in single neurons in acute slice models of ischemia, helps reconcile previous studies focusing primarily on either Ca^{2+} or Zn^{2+}, by clarifying their respective contributions to neuronal death. First, in line with previous observations that persistent high Ca^{2+} rises are linked to irreversible injury (Choi, 1992), we find that the occurrence of Ca^{2+} deregulation during OGD is temporally and causatively linked to a progressive increase in membrane permeability indicative of irreversible neuronal injury [see also Randall and Thayer (1992) and Vander Jagt et al. (2008)]. However, a key new finding of these studies is that somatic Zn^{2+} rises occur distinctly before, and contribute to the occurrence of the Ca^{2+} deregulation. Similar results have also

been observed with NMDA stimulation of CA1 dendrites (Vander Jagt et al., 2009). Other findings indicate that the Zn^{2+} accumulation contributes (along with Ca^{2+}) to the loss of synaptic transmission during acute OGD, and lend support to the idea that mitochondria are important sites of these early Zn^{2+} effects.

Discrimination of Zn^{2+} versus Ca^{2+} rises

The ability of many Ca^{2+} indicators to respond to Zn^{2+} has presented a challenge to efforts to examine changes in Ca^{2+} (as well as Zn^{2+}) during slice OGD, an issue recently highlighted by studies suggesting that Zn^{2+} may actually account for much of the increase in signals of the indicator Calcium Green-1 (Stork and Li, 2006). A recent cell culture study provided precedent for the feasibility of dual indicator imaging to discriminate between Zn^{2+} and Ca^{2+} rises (Devinney et al., 2005), and present results, like another recent slice study (Dietz et al., 2008) support the utility of dual dye loading of single neurons to discriminate Zn^{2+} from Ca^{2+} responses in slice. First, since FluoZin-3 is highly selective for Zn^{2+} (Gee et al., 2002; Devinney et al., 2005), and the FluoZin-3 signal is markedly diminished by TPEN, it seems that the FluoZin-3 signal, which preceded the fura-6F signal is indeed due to Zn^{2+}.

Although fura family indicators can respond to Zn^{2+} as well as to Ca^{2+}, present results further support the contention that most of the fura-6F signals we observe are substantially due to Ca^{2+}. This conclusion is supported by observations that the fura-6F signal (and subsequent membrane permeability increases) is qualitatively unchanged in the presence of TPEN exposures which substantially abolish the FluoZin-3 signal. However, we cannot rule out the possibility that Zn^{2+} could contribute to some of the fura-6F signals, perhaps particularly in the Ca^{2+}-free ACSF experiments when loss of dominant effects of Ca^{2+} binding may reveal a significant contribution of Zn^{2+} to fura signals.

Early interaction of Zn^{2+} with mitochondria during OGD

Prior culture studies have indicated that exogenously applied Zn^{2+} can be taken up into and induce potent effects on mitochondria, including loss of $\Delta\Psi_m$, release of reactive oxygen species (ROS) and of apoptotic mediators (like cytochrome C), and induction of mitochondrial swelling (Sensi et al., 1999; Jiang et al., 2001; Dineley et al., 2005). Subsequent observations that oxidant-induced mobilization of endogenous Zn^{2+} already in neurons also can interfere with mitochondrial function (Sensi et al., 2003; Bossy-Wetzel et al., 2004) further support the idea that mitochondria may be important targets of Zn^{2+} in ischemia. This idea was considerably strengthened by recent *in vivo* ischemia studies in which Zn^{2+} appears to contribute to postischemic mitochondrial dysfunction. Pretreatment of animals with
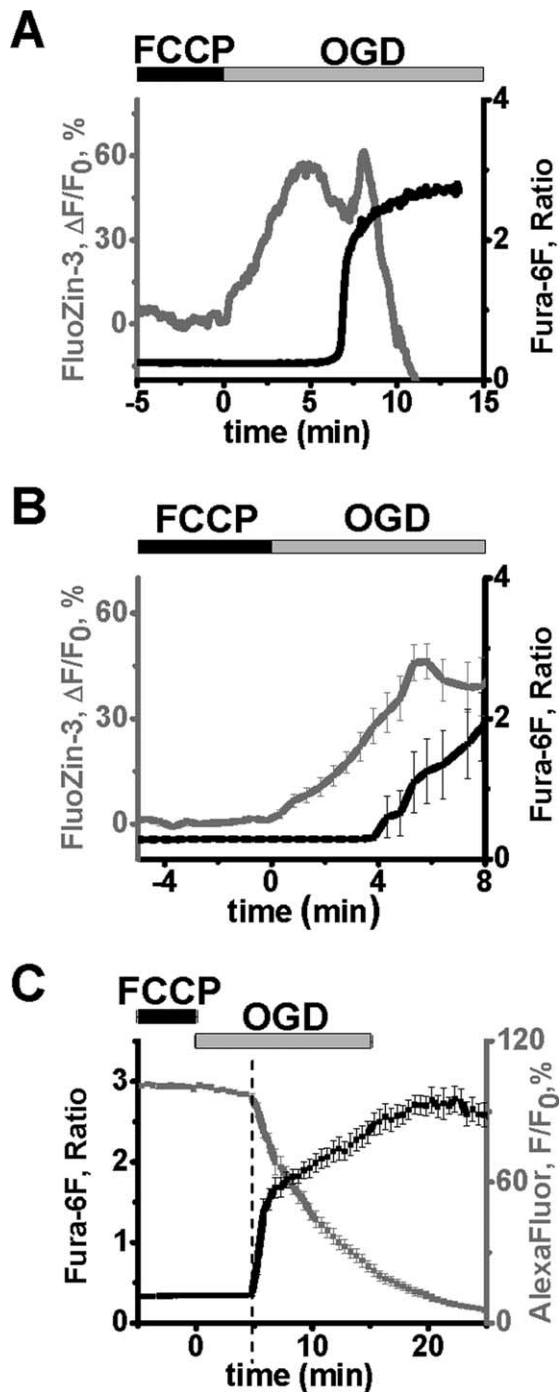
Figure 6. Partial mitochondrial uncoupling results in accelerated OGD-induced Zn^{2+} rises and Ca^{2+} deregulation. Neurons were loaded as indicated and exposed to FCCP (5 μM) for 5 min, followed by 15 min OGD. **A**, Traces from a representative neuron show that both the initial Zn^{2+} rise (gray) and the Ca^{2+} deregulation (black) were substantially accelerated, with the Zn^{2+} rise beginning within the first minute of OGD. **B**, Average traces (±SEM) from 10 CA1 neurons show the Zn^{2+} rise (gray; at $0.79 ± 0.50$ min) and the Ca^{2+} deregulation (black, $5.3 ± 0.38$ min). Data are aligned to the OGD onset to show the start of early $[Zn^{2+}]_i$ rise. **C**, The accelerated OGD-induced Ca^{2+} deregulation after FCCP exposure is still linked to a membrane permeability increase. CA1 neurons were loaded with fura-6F and AlexaFluor-488, and exposed to FCCP before 15 min OGD as above. Traces (±SEM) are aligned to the start of the Ca^{2+} deregulation ($4.9 ± 0.29$ min, $n = 10$ cells).

Figure 7. Zn^{2+} contributes to mitochondrial depolarization during OGD. Slices were bath loaded with the mitochondrial potential ($\Delta\Psi_m$)-sensitive indicator Rhodamine 123 (Rh123), and subjected to 15 min of OGD in the absence or presence of TPEN (40 μM). **A**, Trace shows representative OGD-induced Rh123 fluorescence changes in the CA1 pyramidal cell layer of a control slice (black), and one in which TPEN was present (gray). An increase in fluorescence indicates loss of $\Delta\Psi_m$. **B**, OGD induces a long lasting loss of $\Delta\Psi_m$. After 15 min OGD, slices were allowed to recover for 35 min before exposure to 5 μM FCCP, to directly induce loss of $\Delta\Psi_m$ (peak $\Delta F/F_0$ during OGD, $107 ± 7.35\%$; peak increase after FCCP, $14.1 ± 4.7\%$, $n = 6$). **C**, TPEN improves recovery of $\Delta\Psi_m$ after OGD. Slices were subjected to 15 min OGD as above but in the additional presence of TPEN, and 35 min later exposed to FCCP. The presence of TPEN resulted in a decreased peak $\Delta F/F_0$ during OGD ($73 ± 6.96\%$, $p < 0.01$ vs no TPEN), and an increased response to FCCP ($65.9 ± 7.2\%$, $p < 0.01$ vs no TPEN, $n = 7$), indicating a substantial recovery of $\Delta\Psi_m$ after OGD. In **B** and **C**, traces show mean values ± SEM.

an extracellular Zn^{2+} chelator (Ca-EDTA) decreased cytosolic accumulation of the mitochondrial proapoptotic peptides, cytochrome C and Smac/DIABLO, 12 h after ischemia, and decreased c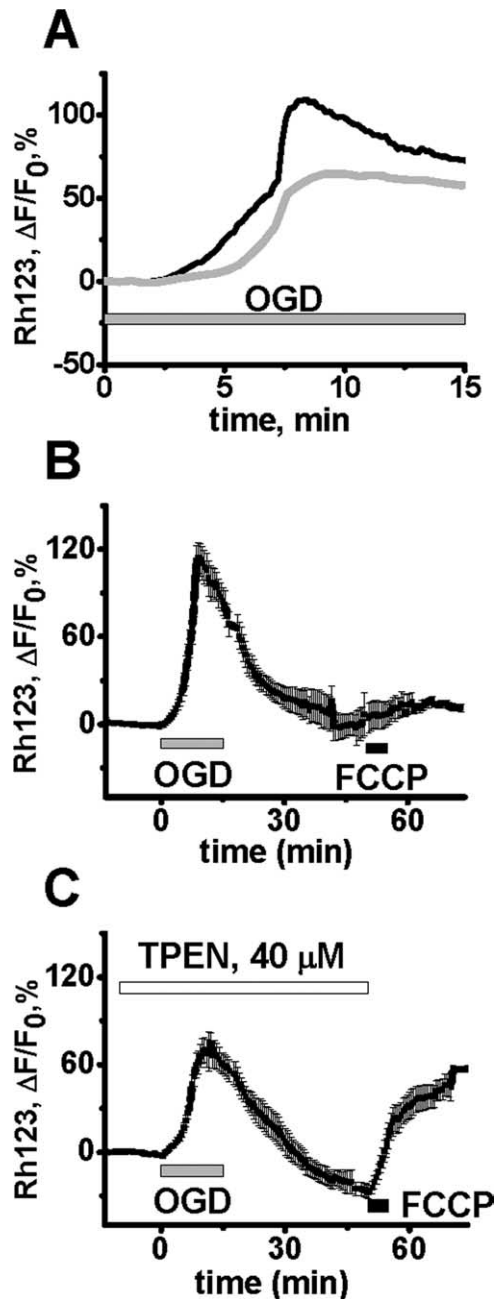onsequent caspase-3 activation (Calderone et al., 2004). Zn^{2+} also appeared to contribute to the appearance of large multiconductance channels in mitochondrial outer membranes 1 h after ischemia via a mechanism involving cleavage of the antiapoptotic BCL-2 family member, BCL-xL (Bonanni et al., 2006).

Present studies extend these observations in two ways. First, they suggest that Zn^{2+}/mitochondria interactions occur very early in simulated ischemia. Indeed, the finding that cytosolic Zn^{2+} accumulation occurs within the first minute of OGD if FCCP is present highlights the rapidity of the Zn^{2+} accumulation and suggests that under normal conditions, Zn^{2+} is taken up by mitochondria and accumulates therein for several minutes before the occurrence of measurable cytosolic Zn^{2+} rises.

Second, the studies suggest that this early Zn^{2+} accumulation, occurring even in the absence of extracellular Ca^{2+}, can trigger a cellular failure which, when sufficiently progressed, results in the occurrence of a lethal Ca^{2+} deregulation event. Although further studies will be necessary to firmly establish the mechanisms of this cellular failure, present studies suggest that mitochondria are likely involved. First, the finding that TPEN enhances recovery of $\Delta\Psi_m$ after OGD indicates that Zn^{2+} contributes to a rapid induction of persistent mitochondrial dysfunction. In addition, although FCCP led to an acceleration of both the early cytosolic Zn^{2+} rise and the Ca^{2+} deregulation, it significantly increased the interval between these events. Thus, present data argue against a predominant contribution of cytosolic Zn^{2+} to the Ca^{2+} deregulation, and favor the idea that intramitochondrial Zn^{2+} plays a role in the triggering of Ca^{2+} deregulation, via a mechanism that may be mimicked by FCCP exposure. Such a role of Zn^{2+} is compatible with previous findings on isolated mitochondria indicating that with nanomolar exposures, Zn^{2+} can enter mitochondria through the Ca^{2+} uniporter, inhibit critical mitochondrial enzymes and induce mitochondrial depolarization and swelling, likely in part via activation of the mitochondrial permeability transition pore (mPTP) (Saris and Niva, 1994; Jiang et al., 2001; Gazaryan et al., 2002, 2007; Sensi et al., 2003; Dineley et al., 2005), and that polarized mitochondria can buffer large Ca^{2+} loads (Werth and Thayer, 1994; Wang and Thayer, 1996).

Synergistic and sequential contributions of Zn^{2+} and Ca^{2+} to ischemic sequelae

Present studies indicate that somatic Zn^{2+} rises precede the Ca^{2+} deregulation, and highlight distinct contributions of each of these ions in the degenerative events. First, chelation studies indicate that Zn^{2+} contributes to the triggering of the terminal Ca^{2+} deregulation. However, as TPEN only delays but does not prevent the Ca^{2+} deregulation (if Ca^{2+} is present) it is apparent that the cellular failure resulting in Ca^{2+} deregulation can be induced by Ca^{2+} in the absence of Zn^{2+}. Conversely, the observation that Zn^{2+} chelation markedly delays terminal Ca^{2+} deregulation after OGD without Ca^{2+} indicates that such failure can also be induced by Zn^{2+} acting largely in the absence of Ca^{2+}. In contrast to the effects of Zn^{2+}, observations that Ca^{2+} deregulation and linked loss of membrane integrity occur only after Ca^{2+} replacement after prolonged OGD indicates that Ca^{2+} plays a critical role in these terminal events, perhaps via activation of Ca^{2+}-dependent catabolic enzymes (Siesjö, 1992). These conclusions as to respective roles of Zn^{2+} and Ca^{2+} are compatible with recent studies of events occurring during prolonged NMDA stimulation of slices (Vander Jagt et al., 2008, 2009).

Studies of the ionic dependence of synaptic failure after OGD show a similar cooperativity of these two ions, with Zn^{2+} removal alone permitting recovery after a shorter OGD (10 min) but combined removal of Zn^{2+} and Ca^{2+} (but not removal of either one alone) permitting recovery after longer (15 min) OGD.

Conclusion/future directions

Present studies provide new insights into the interactions between Zn^{2+} and Ca^{2+} in the triggering of acute ischemic neurodegeneration. Specifically, Zn^{2+} accumulates in neurons soon after the onset of ischemia, is taken up into mitochondria, and contributes to the dysfunction of these organelles as well as to events closely linked to the degenerative process including SD (see Dietz et al., 2008) and Ca^{2+} deregulation. In contrast, the Ca^{2+} deregulation is linked to an increase in membrane permeability.

However, important questions remain. One concerns the sources of the Zn^{2+} and their respective contributions to injury (Weiss et al., 2000; Yin et al., 2002; Lee et al., 2003). Another is the characterization of downstream injury pathways activated after cytosolic Zn^{2+} accumulation. Whereas present studies provide new evidence for a significant early interaction of Zn^{2+} with mitochondria, other studies have implicated diverse mechanisms including NADPH oxidase induction and PARP activation (Kim and Koh, 2002), K^+ current-triggered apoptosis (McLaughlin et al., 2001), and increases in numbers of Ca^{2+}- and Zn^{2+}-permeable AMPA channels (Calderone et al., 2004; Noh et al., 2005) in delayed Zn^{2+}-dependent neurodegeneration. Further understanding of the sources and targets of early Zn^{2+} accumulation and the linkage of these early events to downstream injury mechanisms should suggest improved approaches for ischemic neuroprotection.

References

Arslan P, Di Virgilio F, Beltrame M, Tsien RY, Pozzan T (1985) Cytosolic Ca2+ homeostasis in Ehrlich and Yoshida carcinomas. A new, membrane-permeant chelator of heavy metals reveals that these ascites tumor cell lines have normal cytosolic free Ca2+. J Biol Chem 260:2719–2727.

Bahar S, Fayuk D, Somjen GG, Aitken PG, Turner DA (2000) Mitochondrial and intrinsic optical signals imaged during hypoxia and spreading depression in rat hippocampal slices. J Neurophysiol 84:311–324.

Bonanni L, Chachar M, Jover-Mengual T, Li H, Jones A, Yokota H, Ofengeim D, Flannery RJ, Miyawaki T, Cho CH, Polster BM, Pypaert M, Hardwick JM, Sensi SL, Zukin RS, Jonas EA (2006) Zinc-dependent multiconductance channel activity in mitochondria isolated from ischemic brain. J Neurosci 26:6851–6862.

Bossy-Wetzel E, Talantova MV, Lee WD, Schölzke MN, Harrop A, Mathews E, Götz T, Han J, Ellisman MH, Perkins GA, Lipton SA (2004) Crosstalk between nitric oxide and zinc pathways to neuronal cell death involving mitochondrial dysfunction and p38-activated K(+) channels. Neuron 41:351–365.

Brown AM, Kristal BS, Effron MS, Shestopalov AI, Ullucci PA, Sheu KF, Blass JP, Cooper AJ (2000) Zn2+ inhibits alpha-ketoglutarate-stimulated mitochondrial respiration and the isolated alpha-ketoglutarate dehydrogenase complex. J Biol Chem 275:13441–13447.

Calderone A, Jover T, Mashiko T, Noh KM, Tanaka H, Bennett MV, Zukin RS (2004) Late calcium EDTA rescues hippocampal CA1 neurons from global ischemia-induced death. J Neurosci 24:9903–9913.

Cheng C, Reynolds IJ (1998) Calcium-sensitive fluorescent dyes can report increases in intracellular free zinc concentration in cultured forebrain neurons. J Neurochem 71:2401–2410.

Choi DW (1992) Excitotoxic cell death. J Neurobiol 23:1261–1276.

Devinney MJ 2nd, Reynolds IJ, Dineley KE (2005) Simultaneous detection of intracellular free calcium and zinc using fura-2FF and FluoZin-3. Cell Calcium 37:225–232.

Dietz RM, Weiss JH, Shuttleworth CW (2008) Zn^{2+} influx is critical for some forms of spreading depression in brain slices. J Neurosci 28:8014–8024.

Dineley KE, Votyakova TV, Reynolds IJ (2003) Zinc inhibition of cellular energy production: implications for mitochondria and neurodegeneration. J Neurochem 85:563–570.

Dineley KE, Richards LL, Votyakova TV, Reynolds IJ (2005) Zinc causes loss of membrane potential and elevates reactive oxygen species in rat brain mitochondria. Mitochondrion 5:55–65.

Dohmen C, Sakowitz OW, Fabricius M, Bosche B, Reithmeier T, Ernestus RI, Brinker G, Dreier JP, Woitzik J, Strong AJ, Graf R (2008) Spreading depolarizations occur in human ischemic stroke with high incidence. Ann Neurol 63:720–728.

Duchen MR, Surin A, Jacobson J (2003) Imaging mitochondrial function in intact cells. Methods Enzymol 361:353–389.

Frederickson CJ, Hernandez MD, McGinty JF (1989) Translocation of zinc may contribute to seizure-induced death of neurons. Brain Res 480:317–321.

Gazaryan IG, Krasnikov BF, Ashby GA, Thorneley RN, Kristal BS, Brown AM (2002) Zinc is a potent inhibitor of thiol oxidoreductase activity and stimulates reactive oxygen species production by lipoamide dehydrogenase. J Biol Chem 277:10064–10072.

Gazaryan IG, Krasinskaya IP, Kristal BS, Brown AM (2007) Zinc irreversibly damages major enzymes of energy production and antioxidant defense prior to mitochondrial permeability transition. J Biol Chem 282:24373–24380.

Gee KR, Zhou ZL, Ton-That D, Sensi SL, Weiss JH (2002) Measuring zinc in living cells. A new generation of sensitive and selective fluorescent probes. Cell Calcium 31:245–251.

Hoskison MM, Shuttleworth CW (2006) Microtubule disruption, not calpain-dependent loss of MAP2, contributes to enduring NMDA-induced dendritic dysfunction in acute hippocampal slices. Exp Neurol 202:302–312.

Jiang D, Sullivan PG, Sensi SL, Steward O, Weiss JH (2001) $Zn(2+)$ induces permeability transition pore opening and release of pro-apoptotic peptides from neuronal mitochondria. J Biol Chem 276:47524–47529.

Kim YH, Koh JY (2002) The role of NADPH oxidase and neuronal nitric oxide synthase in zinc-induced poly(ADP-ribose) polymerase activation and cell death in cortical culture. Exp Neurol 177:407–418.

Koh JY, Suh SW, Gwag BJ, He YY, Hsu CY, Choi DW (1996) The role of zinc in selective neuronal death after transient global cerebral ischemia. Science 272:1013–1016.

Lee JY, Kim JH, Palmiter RD, Koh JY (2003) Zinc released from metallothionein-iii may contribute to hippocampal CA1 and thalamic neuronal death following acute brain injury. Exp Neurol 184:337–347.

Link TA, von Jagow G (1995) Zinc ions inhibit the QP center of bovine heart mitochondrial bc1 complex by blocking a protonatable group. J Biol Chem 270:25001–25006.

Lipski J, Park TI, Li D, Lee SC, Trevarton AJ, Chung KK, Freestone PS, Bai JZ (2006) Involvement of TRP-like channels in the acute ischemic response of hippocampal CA1 neurons in brain slices. Brain Res 1077:187–199.

Lobner D, Lipton P (1993) Intracellular calcium levels and calcium fluxes in the CA1 region of the rat hippocampal slice during *in vitro* ischemia: relationship to electrophysiological cell damage. J Neurosci 13:4861–4871.

Manev H, Kharlamov E, Uz T, Mason RP, Cagnoli CM (1997) Characterization of zinc-induced neuronal death in primary cultures of rat cerebellar granule cells. Exp Neurol 146:171–178.

McLaughlin B, Pal S, Tran MP, Parsons AA, Barone FC, Erhardt JA, Aizenman E (2001) p38 activation is required upstream of potassium current enhancement and caspase cleavage in thiol oxidant-induced neuronal apoptosis. J Neurosci 21:3303–3311.

Nicholls DG, Budd SL (2000) Mitochondria and neuronal survival. Physiol Rev 80:315–360.

Noh KM, Yokota H, Mashiko T, Castillo PE, Zukin RS, Bennett MV (2005) Blockade of calcium-permeable AMPA receptors protects hippocampal neurons against global ischemia-induced death. Proc Natl Acad Sci U S A 102:12230–12235.

Randall RD, Thayer SA (1992) Glutamate-induced calcium transient triggers delayed calcium overload and neurotoxicity in rat hippocampal neurons. J Neurosci 12:1882–1895.

Rothman SM, Olney JW (1986) Glutamate and the pathophysiology of hypoxic–ischemic brain damage. Ann Neurol 19:105–111.

Saris NE, Niva K (1994) Is Zn2+ transported by the mitochondrial calcium uniporter? FEBS Lett 356:195–198.

Sensi SL, Yin HZ, Carriedo SG, Rao SS, Weiss JH (1999) Preferential Zn2+ influx through Ca2+-permeable AMPA/kainate channels triggers prolonged mitochondrial superoxide production. Proc Natl Acad Sci U S A 96:2414–2419.

Sensi SL, Ton-That D, Weiss JH (2002) Mitochondrial sequestration and $Ca(2+)$-dependent release of cytosolic $Zn(2+)$ loads in cortical neurons. Neurobiol Dis 10:100–108.

Sensi SL, Ton-That D, Sullivan PG, Jonas EA, Gee KR, Kaczmarek LK, Weiss JH (2003) Modulation of mitochondrial function by endogenous Zn2+ pools. Proc Natl Acad Sci U S A 100:6157–6162.

Shuttleworth CW, Connor JA (2001) Strain-dependent differences in calcium signaling predict excitotoxicity in murine hippocampal neurons. J Neurosci 21:4225–4236.

Siesjö BK (1988) Historical overview. Calcium, ischemia, and death of brain cells. Ann N Y Acad Sci 522:638–661.

Siesjö BK (1992) Pathophysiology and treatment of focal cerebral ischemia. Part II: Mechanisms of damage and treatment. J Neurosurg 77:337–354.

Skulachev VP, Chistyakov VV, Jasaitis AA, Smirnova EG (1967) Inhibition of the respiratory chain by zinc ions. Biochem Biophys Res Commun 26:1–6.

Stork CJ, Li YV (2006) Intracellular zinc elevation measured with a "calcium-specific" indicator during ischemia and reperfusion in rat hippocampus: a question on calcium overload. J Neurosci 26:10430–10437.

Tanaka E, Yamamoto S, Kudo Y, Mihara S, Higashi H (1997) Mechanisms underlying the rapid depolarization produced by deprivation of oxygen and glucose in rat hippocampal CA1 neurons in vitro. J Neurophysiol 78:891–902.

Tønder N, Johansen FF, Frederickson CJ, Zimmer J, Diemer NH (1990) Possible role of zinc in the selective degeneration of dentate hilar neurons after cerebral ischemia in the adult rat. Neurosci Lett 109:247–252.

Vander Jagt TA, Connor JA, Shuttleworth CW (2008) Localized loss of Ca^{2+} homeostasis in neuronal dendrites is a downstream consequence of metabolic compromise during extended NMDA exposures. J Neurosci 28:5029–5039.

Vander Jagt TA, Connor JA, Weiss JH, Shuttleworth CW (2009) Intracellular Zn2+ increases contribute to the progression of excitotoxic Ca2+ increases in apical dendrites of CA1 pyramidal neurons. Neuroscience. Advance online publication. Retrieved January 19, 2009. doi:10.1016/j.neuroscience.2008.11.052.

Wang GJ, Thayer SA (1996) Sequestration of glutamate-induced Ca2+ loads by mitochondria in cultured rat hippocampal neurons. J Neurophysiol 76:1611–1621.

Wei G, Hough CJ, Li Y, Sarvey JM (2004) Characterization of extracellular accumulation of Zn2+ during ischemia and reperfusion of hippocampus slices in rat. Neuroscience 125:867–877.

Weiss JH, Sensi SL, Koh JY (2000) $Zn(2+)$: a novel ionic mediator of neural injury in brain disease. Trends Pharmacol Sci 21:395–401.

Werth JL, Thayer SA (1994) Mitochondria buffer physiological calcium loads in cultured rat dorsal root ganglion neurons. J Neurosci 14:348–356.

Yin HZ, Sensi SL, Ogoshi F, Weiss JH (2002) Blockade of Ca^{2+}-permeable AMPA/kainate channels decreases oxygen-glucose deprivation-induced Zn^{2+} accumulation and neuronal loss in hippocampal pyramidal neurons. J Neurosci 22:1273–1279.